TRENDS IN SCIENCES 2026; 23(9): 13059
https://doi.org/10.48048/tis.2026.13059 RESEARCH ARTICLE

# Cytotoxicity Evaluation of Silver Nanoparticles Synthesized Using Ethanol Extract of White Galangal (*Alpinia galanga*) Rhizome against Liver Cancer Cell Line (Huh7it): An *In Vitro* and *In Silico* Study

**Rr Aulia Rahmawati Kusuma Putri[1], Mochammad Aqilah Herdiansyah[1], Aulia Umi Rohmatika[2], Sri Rahayu[3] and Win Darmanto[1,*]**

[1]*Department of Biology, Faculty of Science and Technology, Universitas Airlangga, East Java, Indonesia*
[2]*Faculty of Medicine, Universitas Pembangunan Nasional Veteran Jawa Timur, East Java, Indonesia*
[3]*Department of Biology, Faculty of Mathematics and Natural Sciences, Universitas Brawijaya, East Java, Indonesia*

**([*]Corresponding author's e-mail: windarmanto@fst.unair.ac.id)**

*Received: 16 December 2025, Revised: 18 January 2026, Accepted: 28 January 2026, Published: 1 April 2026*

**Abstract**

Liver cancer remains one of the leading causes of cancer deaths worldwide, with hepatocellular carcinoma being the most commonly occurring form. In an attempt to find safe and effective alternative therapies, this study assessed the anti-cancer potential of ethanol-based silver nanoparticles synthesized from *Alpinia galanga* rhizomes (white galangal) (AgNPs-AG). The metabolite profile of the ethanol extract, analyzed by LC-MS, identified 20 major compounds, among which 2,3-Dihydroxybenzoylserine emerged as the top anticancer candidate (Pa = 0.383) based on PASS prediction. Green synthesis of silver nanoparticles was successfully achieved using the extract as a reducing and stabilizing agent.

Comprehensive characterization confirmed the formation of stable silver nanoparticles. UV-Vis spectroscopy showed a characteristic surface plasmon resonance peak at 420 nm, while FT-IR analysis revealed the presence of –OH and C=O functional groups that functioned as capping agents. Particle size analysis showed an average size of 6.35 nm with a uniform distribution, and a zeta potential of –28.6 mV indicated good colloidal stability. Further *in silico* molecular docking supports the anticancer potential of 2,3-Dihydroxybenzoylserine, which shows strong binding to Caspase-9 (–7.3 kcal/mol), implying intrinsic apoptosis pathway activation.

*In vitro* toxicity was evaluated using the Huh7it hepatocellular carcinoma cell line. Treatment with AgNPs-AG at concentrations ranging from 6.25 to 200 µg/mL for 24 and 48 h of incubation caused a decrease in cell viability, depending on the dose and time. The $IC_{50}$ values obtained were 71.046 µg/mL (24 h) and 63.395 µg/mL (48 h), indicating increased cytotoxicity with longer exposure. Collectively, findings highlight the encouraging potential of AgNPs-AG as a novel candidate for liver cancer therapy.

**Keywords:** *Alpinia galanga*, Green synthesis, Hepatocellular carcinom, LC-MS, Molecular docking

## Introduction

Liver cancer is one of the leading causes of cancer deaths worldwide and continues to show an increase in incidence each year. Hepatocellular carcinoma (HCC), the most common form of primary liver cancer, accounts for more than 75% - 85% of cases and ranks sixth among the most common cancers and third among causes of cancer deaths globally [1]. It is estimated that there are approximately 600,000 - 800,000 new cases of HCC each year, and this number could reach one million cases by 2030 if there are no effective interventions [2]. The main risk factors contributing to the increase in HCC cases include chronic hepatitis B and C infections, alcohol-induced cirrhosis, and metabolic diseases such as NAFLD and NASH, whose prevalence has increased significantly in the last decade [3].

Signaling pathways are important, especially the EGFR/PI3K/Akt pathway, which plays a role in the

growth, invasion, and resistance of cancer cells to apoptosis [4]. EGFR overexpression is detected in more than 60% of HCC cases and is closely related to tumor aggressiveness [5]. Overexpression of this pathway is often triggered by epigenetic changes, such as MIG6 hypermethylation, which eliminates its inhibitory function on EGFR, thereby triggering hyperactivation of the ERK/Akt/mTOR pathway [6,7]. Additionally, the accumulation of reactive oxygen species (ROS) due to viral infection or chronic cellular stress accelerates DNA damage and facilitates tumor development [8,9]. This combination of dysregulation contributes to resistance to conventional therapy and the high incidence of HCC.

*Alpinia galanga* (white galangal) is a medicinal plant widely used in traditional medicine and is rich in bioactive metabolites, including phenolics, flavonoids, and terpenoids, which have been reported to exhibit antioxidant, anti-inflammatory, and anticancer properties [10,11]. Several compounds from A. galanga, such as galangin and acetoxychavicol acetate (ACA), have demonstrated antiproliferative activity in various cancer models, mainly through modulation of apoptosis- and cell cycle–related pathways [12,13].

The green synthesis of silver nanoparticles (AgNPs) using plant extracts has emerged as a promising strategy to enhance the biological activity of phytochemicals. Biosynthesized AgNPs exhibit notable anticancer effects, primarily through oxidative stress induction and apoptosis-related mechanisms, while offering improved biocompatibility and environmental safety compared to chemically synthesized nanoparticles [14]. Previous studies have shown that silver nanoparticles derived from *Alpinia* species possess cytotoxic activity against several human cancer cell lines, supporting their potential as anticancer agents [15].

In addition to *in vitro* approaches, *in silico* analyses such as molecular docking provide important mechanistic information for predicting molecular interactions between the active compounds of *A. galanga* and cancer target proteins, including EGFR, p53, caspase-9, and CDK4, which play central roles in proliferation and apoptosis pathways [16]. The integration of experimental and computational approaches strengthens the understanding of an agent's anticancer potential before proceeding to further drug development stages.

Although several studies have reported the green synthesis of silver nanoparticles using *Alpinia* species, most of these studies have primarily focused on nanoparticle synthesis and general cytotoxic effects on various cancer cell lines. Studies specifically exploring *A. galanga*-mediated silver nanoparticles in the context of hepatocellular carcinoma, particularly with mechanistic insights related to EGFR/PI3K/Akt signaling and apoptosis-related targets, remain limited. Furthermore, the integration of phytochemical-based green synthesis with *in vitro* cytotoxic evaluation and *in silico* molecular interaction analysis has not been widely reported. Therefore, this study aims to fill this gap by investigating the anticancer potential of silver nanoparticles derived from *A. galanga* against HCC cells using experimental and computational approaches.

This study aims to evaluate the cytotoxicity of silver nanoparticles synthesized using ethanol extract of white galangal rhizome (*A. galanga*) (AgNPs-AG) against hepatocellular carcinoma Huh7it cells *in vitro*, as well as predict their molecular interactions through an *in-silico* approach.

## Materials and methods

### Plant material and ethanol extract preparation

Fresh *Alpinia galanga* rhizomes were collected from Kediri City, East Java, Indonesia. The parts of the plant used included the base of the stem near the rhizome, which is white, to the middle part of the stem, which is light green. The plant material was washed, sliced, and dried at room temperature, then dried in an oven at 38 °C to ensure the removal of residual moisture. The dried stems were then ground to obtain 100 g of fine powder [17]. Extraction was carried out using the maceration method, which involved soaking 100 g of powder in 1,000 mL of 70% ethanol (1:10 w/v) for 72 h while stirring occasionally. After filtration, the plant residue was macerated again in the same volume of solvent for 24 h. The 2 filtrates were combined and evaporated using an oven at 50 °C and a water bath until a thick extract was obtained. The extract was then stored in a closed container and protected from light to prevent photodegradation of phytochemical compounds [17,18]. Extraction conditions have been standardized and applied consistently to enable reproducibility.

**LC-MS analysis**

The phytochemical profile of *A. galanga* ethanol extract was analyzed using a Vanquish UHPLC system connected to a Q Exactive Plus Orbitrap HRMS (Thermo Scientific). Chromatographic separation was performed using an Accucore C18 column (100×2.1 $mm^2$; 1.5 µm). The mobile phase consisted of water with 0.1% formic acid (eluent A) and acetonitrile with 0.1% formic acid (eluent B). The elution gradient started from 5% to 95% eluent B for 25 min, was maintained for 3 min, and returned to the initial condition until the 33rd min. The flow rate was set at 0.2 mL/min, column temperature at 30 °C, and injection volume at 2 µL. Detection was performed using Heated Electrospray Ionization (HESI) in positive and negative modes with a mass range of m/z 100 - 1,500 and a resolution of 70,000 for full MS and 17,500 for dd-$MS^2$. Other parameters included a spray voltage of 3.80 kV, a capillary temperature of 320 °C, a shroud gas flow rate of 15, an auxiliary gas flow rate of 2, a sweep gas flow rate of 0, and an S-lens RF of 50. The data were analyzed using the instrument's built-in software, and the compounds were tentatively identified using the mzCloud and ChemSpider databases.

**Synthesis of silver nanoparticles (AgNPs)**

Green synthesis of AgNPs was carried out using ethanol extract of *A. galanga* as a natural reducing agent and stabilizer. A total of 0.02 g of concentrated extract was dissolved in 5 mL of distilled water and stirred at 60 °C for 5 minutes at 100 rpm. After that, 5 mL of 0.1 M $AgNO_3$ solution was added and the mixture was stirred again for 5 min at 1,000 rpm with the temperature maintained at 60 °C. A brown color change indicated the formation of silver nanoparticles. The reaction mixture was then stirred at 30 °C for 15 min at 100 rpm, and the pH was adjusted to 7. The AgNPs suspension was then frozen and dried using a freeze-dryer to obtain dry nanoparticles, which were stored at 4 °C for further analysis.

**Characterization of Silver Nanoparticles**

The formation and optical properties of AgNPs were confirmed using a UV–Vis spectrophotometer by scanning the sample at wavelengths of 300 - 700 nm to detect the surface plasmon resonance peak characteristic of silver nanoparticles [19]. Furthermore, analysis of functional groups was performed using Fourier Transform Infrared Spectroscopy (FTIR) to identify biomolecules involved in the reduction and capping processes. Dried AgNPs samples were mixed with KBr and pressed into pellets, then scanned in the wavenumber range of 4,000 - 400 $cm^{-1}$ with a resolution of 1 $cm^{-1}$ using the KBr pellet method [19]. Particle size, hydrodynamic diameter, polydispersity index (PDI), and zeta potential were determined using Dynamic Light Scattering (DLS) with a He–Ne laser (633 nm). The sample was diluted two to three times using deionized water to obtain optimal scattering intensity [19,20]. The surface morphology and structural characteristics of AgNPs were analyzed using Scanning Electron Microscopy (SEM). Droplests of nanoparticle suspension were placed on a stainless steel holder, dried at room temperature, coated with a thin layer of gold using a sputter coater, and observed at an operating voltage of 16 kV with various magnification levels [21,22].

**Cell culture and cytotoxicity assay**

Human liver cancer cells (Huh7it) were cultured in Petri dishes using Dulbecco's Modified Eagle Medium (DMEM; Invitrogen, Carlsbad, CA, USA) supplemented with 10% fetal bovine serum (FBS; Biowest, Nuaille, France), kanamycin (150 µg/mL; Sigma-Aldrich), and nonessential amino acids (Invitrogen). Cells were maintained in a humidified incubator at 37 °C with 5% $CO_2$ [23]. The cytotoxicity assay was performed using the MTT method. Huh7it cells were seeded in a 96-well microplate at a density of $2.4\times10^4$ cells per welland incubated for 24 h to allow the cells to adapt. After that, the cells were treated with AgNPs at concentrations of 6.25, 12.5, 25, 50, 100 and 200 µg/mL. This concentration range was selected to generate a dose-response curve and enable the determination of $IC_{50}$. Untreated cells were used as negative controls, while 10 µg/mL doxorubicin treatment was used as a positive control. The treatments were administered for 24 and 48 h. All treatments were performed in triplicate. Following treatment, the culture medium was discarded and replaced with 150 µL of fresh DMEM containing 0.5 mg/mL MTT solution, then incubated for 4 h at 37 °C until formazan crystals were formed. The medium was subsequently removed, and 100 µL of dimethyl sulfoxide (DMSO) was added to

dissolve the formazan crystals. Absorbance was measured at 560 nm with a reference wavelength of 750 nm using a GloMax-Multi Microplate Multimode Reader (Promega). Cell viability was calculated relative to the untreated control [23].

***In silico* analysis**

***Pharmacokinetic and ADMET prediction***

Pharmacokinetic and ADMET analyses were performed using SwissADME and pkCSM. The SMILES structures of compounds identified by LC-MS were obtained from PubChem and entered into SwissADME to assess physicochemical properties, lipophilicity, solubility, and pharmacokinetic parameters. ADMET prediction was performed using pkCSM by entering the SMILES code [24].

***Ligand and target protein preparation***

Compounds in .sdf format from PubChem were converted to .pdb format using PyMOL, then energy minimization was performed using Open Babel in PyRx 0.8 [25]. The structures of protein targets relevant to liver cancer, namely EGFR (PDB: 3NJP), TP53 (PDB: 1TUP), caspase-9 (PDB: 2AR9), and CDK4 (PDB: 6P8F), were downloaded from the RCSB Protein Data Bank. Crystal water molecules and non-essential atoms were removed, and the structures were saved in.pdbqt format for the docking process [24,26].

**Molecular docking**

Docking was performed using AutoDock Vina on PyRx 0.8. The grid box was adjusted to cover the active sites of each protein, and exhaustiveness was set to a value of 8 to improve accuracy. The pose with the lowest binding affinity value was selected as the best result. Ligand-protein interactions were visualized using LigPlot+ and BIOVIA Discovery Studio to identify hydrogen bonds, hydrophobic interactions, and electrostatic interactions [24,27].

**Statistical analysis**

All data are presented as mean ± standard deviation (SD). Statistical analysis was performed using 1-way ANOVA followed by Tukey's post hoc test, with $p < 0.05$ considered statistically significant. $IC_{50}$ values were calculated using GraphPad Prism 9. Binding affinity parameters and ADMET results were analyzed descriptively.

## Results and discussion

**Metabolite profile of *Alpinia galanga* ethanol extract**

LC-MS analysis identified 20 metabolite compounds in the ethanol extract of *Alpinia galanga* rhizome with a wide range of polarity as shown in **Figure 1** and **Table 1**. The compounds with the highest intensity were DL-malic acid (RT 1.12; area $5.31\times10^9$), followed by D-(+)-galactose (RT 1.09; area $3.94\times10^9$), choline (RT 1.04), and piclamilast (RT 1.04). The predominance of these polar metabolites indicates the extract's strong potential as a bioreductant and natural capping agent in silver nanoparticle synthesis. In particular, DL-malic acid together with citric acid (RT 1.11) has been reported to reduce $Ag^+$ ions and maintain nanoparticle stability and size through the formation of dicarboxylate complexes [28-30]. Malic acid and citric acid play an important role in cellular energy metabolism. In cancer cells, citric acid metabolism disorders are often associated with increased glycolysis and proliferation. The administration of this organic compound can restore redox balance and inhibit tumor growth through antimetabolic effects [31].

**Table 1** Identification of secondary metabolite compounds in the ethanol extract of *A. galanga* rhizomes using LC-MS.

| No | Compound Name | Molecular Formula | Sample Area | RT (min) |
|---|---|---|---|---|
| 1 | DL-Malic acid | $C_4H_6O_5$ | $5.31\times10^9$ | 1.12 |
| 2 | D-(+)-Galactose | $C_6H_{12}O_6$ | $3.94\times10^9$ | 1.09 |
| 3 | Choline | $C_5H_{13}NO$ | $2.85\times10^9$ | 1.04 |
| 4 | Cinnamaldehyde | $C_9H_8O$ | $1.99\times10^9$ | 15.33 |
| 5 | Citric acid | $C_6H_8O_7$ | $4.47\times10^8$ | 1.11 |

| No | Compound Name | Molecular Formula | Sample Area | RT (min) |
|---|---|---|---|---|
| 6 | 2,3-Dihydroxybenzoylserine (DHBS) | $C_{10}H_{11}NO_6$ | $1.49\times10^8$ | 3.23 |
| 7 | Hexahydrocurcumin (HHC) | $C_{21}H_{26}O_6$ | $2.19\times10^8$ | 15.07 |
| 8 | N-Acetylneuraminic acid (Sialic acid) | $C_{11}H_{19}NO_9$ | $3.43\times10^8$ | 1.09 |
| 9 | Alpha-Naphthoflavone | $C_{19}H_{12}O_2$ | $1.72\times10^8$ | 19.2 |
| 10 | Phenprocoumon | $C_{18}H_{16}O_3$ | $1.38\times10^8$ | 13.92 |
| 11 | Piclamilast | $C_{18}H_{18}Cl_2N_2O_3$ | $2.02\times10^9$ | 1.04 |
| 12 | 2-C-methylerythritol 4-phosphate | $C_5H_{13}O_7P$ | $1.50\times10^9$ | 1 |
| 13 | N-Glycosyl-L-asparagine | $C_{10}H_{18}N_2O_8$ | $1.50\times10^9$ | 1.04 |
| 14 | (9Z)-9-Octadecenamide | $C_{18}H_{35}NO$ | $1.25\times10^9$ | 25.46 |
| 15 | N-ethylmaleimide | $C_6H_7NO_2$ | $1.14\times10^9$ | 1.1 |
| 16 | 4-Aminobenzoic acid | $C_7H_7NO_2$ | $7.46\times10^8$ | 1.08 |
| 17 | Diacetin | $C_7H_{12}O_5$ | $5.78\times10^8$ | 5.49 |
| 18 | Guaietolin | $C_{11}H_{16}O_4$ | $4.12\times10^8$ | 14.03 |
| 19 | D-Glucono-δ-lactone | $C_6H_{10}O_6$ | $3.99\times10^8$ | 1.23 |
| 20 | L-(+)-Valine | $C_5H_{11}NO_2$ | $4.70\times10^8$ | 1.06 |

Medium to high RT detected several phenolic compounds, particularly cinnamaldehyde (RT 15.33) is known as a phenylpropane compound that can induce apoptosis in cancer cells by increasing reactive oxygen species and activating the caspase pathway. In addition, cinnamaldehyde suppresses cancer cell proliferation by inhibiting the expression of NF-κB and Bcl-2 [32-34]. Hexahydrocurcumin (RT 15.07), a reduced derivative of curcumin, is also known to exhibit anticancer effects through the induction of autophagy and apoptosis, as well as the inhibition of the PI3K/Akt/mTOR pathway, which plays a role in cancer proliferation [35]. These findings support the cytotoxic mechanism observed in Huh7it cells in the MTT assay. Another important compound that was also analyzed further through docking was 2,3-dihydroxybenzoylserine (DHBS) (RT 3.23; area $1.49\times10^8$). The catechol group in DHBS functions as a reducing agent and metal chelator that increases the stability of AgNPs [36], while also increasing oxidative stress and apoptosis [30], making it a prime candidate in the evaluation of interactions with p53, caspase-9, EGFR, and CDK4.

In addition, LC-MS also identified metabolites that support specific hepatocyte targeting, such as D-galactose (ASGPR-mediated uptake) and N-acetylneuraminic acid (sialic acid) (RT 1.09), which enhance nanoparticle internalization in HCC cells [37-39]. The compound N-glycosyl-L-asparagine (RT 1.04) carries an NGR motif that binds to the CD13 receptor on cancer cells [40], thereby supporting the AgNPs targeting mechanism in Huh7it cells.

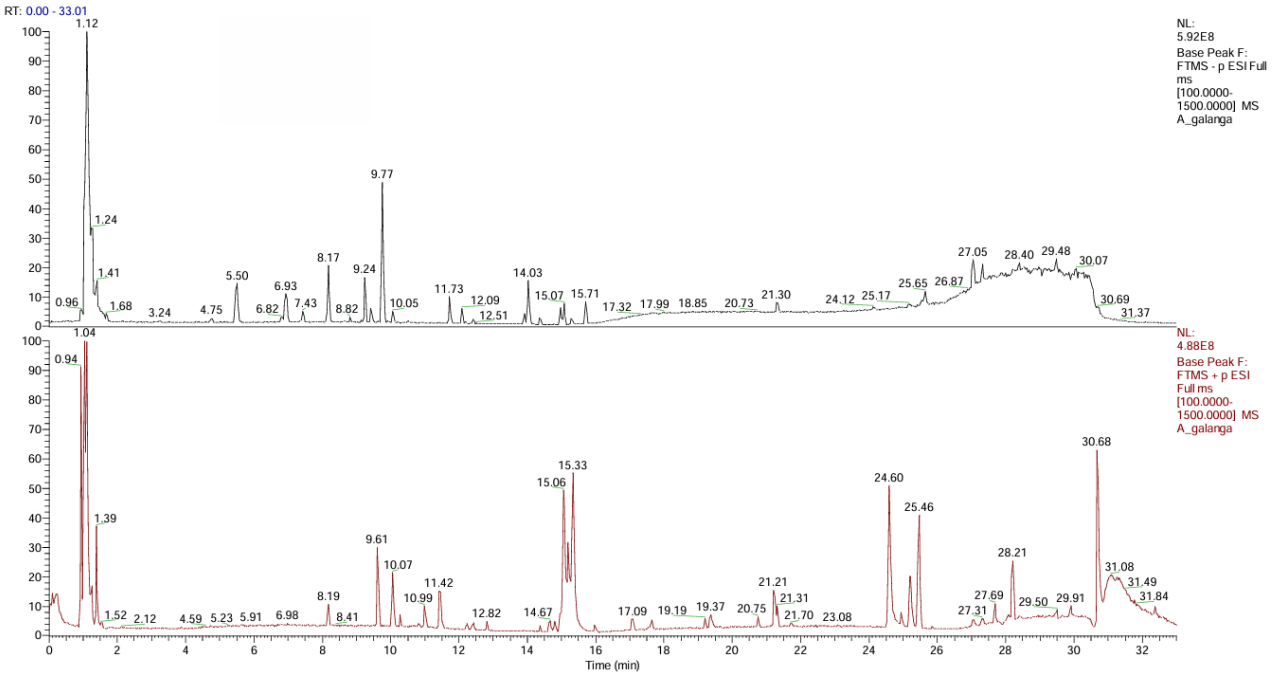


**Figure 1** LC-MS chromatogram of the ethanol extract of *A. galanga* rhizome, showing the detected phytochemical constituents used as reducing and stabilizing agents in the green synthesis of silver nanoparticles.

Other metabolites relevant to proliferation and oxidative stress pathways were also detected, such as alpha-naphthoflavone (RT 19.20) as a CYP1A1/1A2 inhibitor [41], 4-aminobenzoic acid as a Wnt/β-catenin inhibitor [42], N-ethylmaleimide as a ROS inducer [43], and L-valine which enhances nanoparticle internalization via the LAT1 transporter [44]. Meanwhile, (9Z)-9-octadecenamide (RT 25.46), one of the compounds also used in docking, exhibits a strong lipophilic profile and has been associated with antiproliferative activity but has low permeability [45]. Previously, this compound was known to have antiproliferative and anti-inflammatory effects through modulation of cannabinoid receptors and MAPK signaling pathways, which contribute to cytotoxic effects on several cancer cells [46].

**Characterization of AgNPs-AG**

***Synthesis and UV-Vis spectrum***

The synthesis process of silver nanoparticles using *A. galanga* extract is characterized by a change in the color of the solution from clear ($AgNO_3$) to yellow and then golden brown. This change is a visual indication of the formation of silver nanoparticles and is related to the phenomenon of surface plasmon resonance (SPR), which is the oscillation of free electrons on the surface of metal nanoparticles when exposed to visible light [47]. These results are consistent with the synthesis of AgNPs based on *A. galanga* methanol extract, which also showed a gradual color change as the reduction progressed [19]. Pure $AgNO_3$ solution only showed low absorbance without an SPR peak, while *A. galanga* extract displayed a characteristic absorption pattern of organic compounds without any indication of nanoparticle formation. These findings confirm that the reduction of $Ag^+$ to $Ag^0$ occurs when bioactive compounds from *A. galanga* extract act as reducing agents and stabilizers in the nanoparticle synthesis process [48].

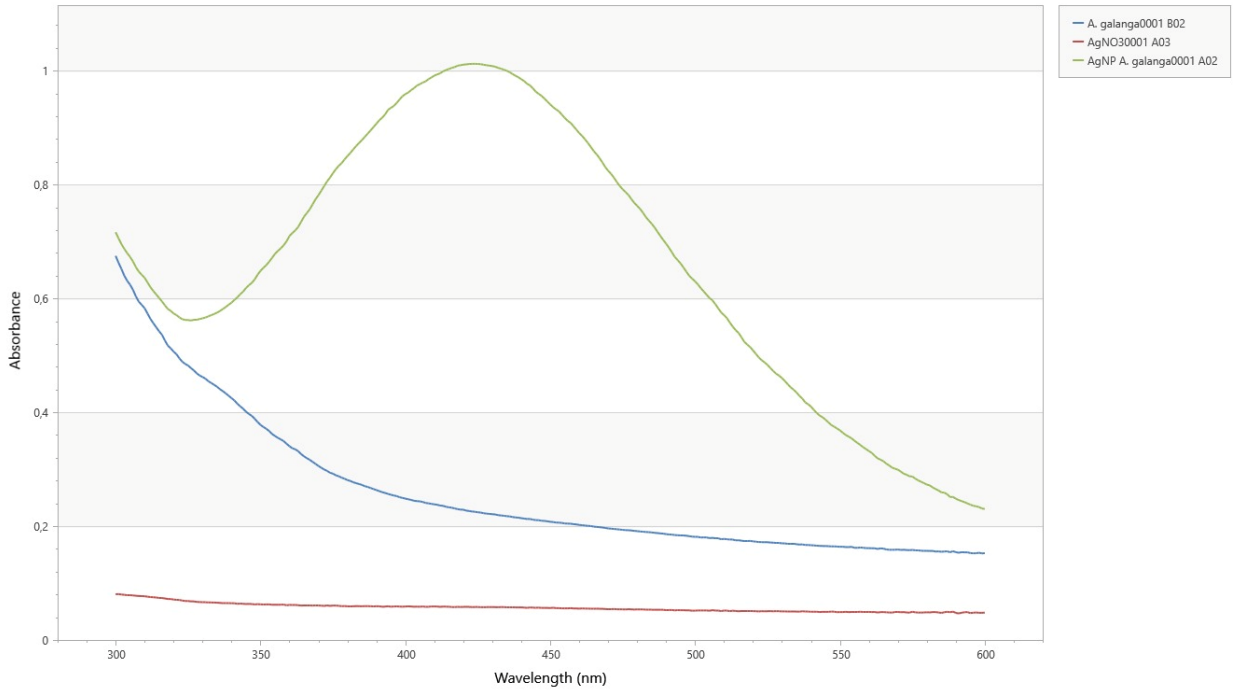


**Figure 2** UV-Vis absorption spectra of the ethanol extract of *A. galanga* rhizome (blue), $AgNO_3$ solution (red), and biosynthesized silver nanoparticles (AgNPs-AG, green) recorded in the wavelength range of 300 - 600 nm. The characteristic surface plasmon resonance peak confirms the formation of AgNPs-AG.

The UV-Vis spectrum shows the maximum absorption peak of silver nanoparticles at around 420 nm with a higher intensity than $AgNO_3$ solution or pure extract (**Figure 2**). This peak is a characteristic of silver nanoparticle SPR, which generally appears in the range of 300 - 600 nm [48]. Research by Imchen *et al.* [45] also reported absorption peaks at 417 - 423 nm for AgNPs biosynthesized using extracts from *A. galanga* rhizomes and Rhus semialata fruit. The increase in peak intensity at 420 nm in this study indicates that the reduction process was efficient and produced a significant amount of AgNPs with good optical stability [50].

***Particle size, distribution, and zeta potential***

PSA analysis shows that AgNPs-AG has an average size of 6.35 nm with a PDI of 0.2347 and D10, D50, and D90 values of 2.45, 4.41, and 7.96 nm, respectively (**Figure 3**). This distribution indicates that approximately 90% of the particles are below 8 nm and have good size homogeneity [51]. The PDI value obtained is in line with the results of Ahmad *et al.* [19], who reported a PDI value of 0.24. This ultra-small size increases the specific surface area and accelerates the release of $Ag^+$ ions, thereby strengthening interactions with cell membranes and intracellular components and inducing oxidative stress that plays a role in cytotoxic mechanisms [52]. These findings are consistent with reports by Rodríguez-Félix *et al.* [53]; Hemmati *et al.* [54], which show that plant-biosynthesized AgNPs are generally 5 - 10 nm in size with a narrow distribution and high biological activity.

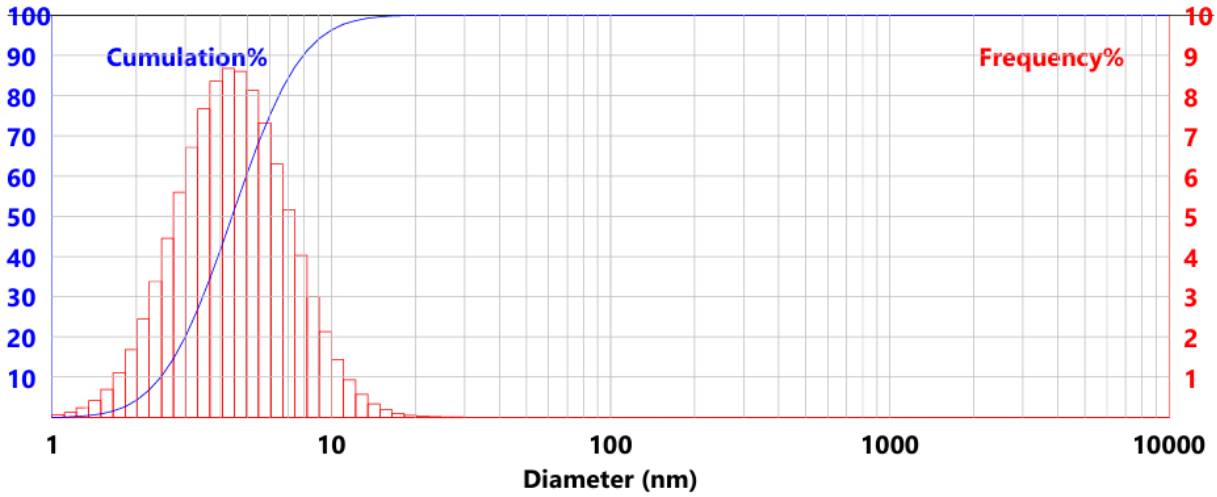


**Figure 3** Particle size distribution of AgNPs-AG determined by particle size analysis (PSA), showing the nanoscale size range of the synthesized silver nanoparticles.

Zeta potential measurements indicate that AgNPs-AG has a value of –29.58 ± 5.45 mV (**Figure 4**), which indicates good colloidal stability due to the presence of electrostatic repulsive forces between particles [55]. Nanoparticles with a zeta potential ≥ ± 30 mV are generally stable in liquid media [55], and a range of –19 to –44 mV has been widely reported in biosynthetic silver nanoparticles [56,57]. This negative charge is thought to originate from the adsorption of nitrate ions and negatively charged organic compounds on the nanoparticle surface. In addition to maintaining colloidal stability, this negative charge also enhances electrostatic interactions with cancer cell membranes, which tend to be positively charged, thereby accelerating AgNPs internalization and strengthening oxidative stress induction [58].

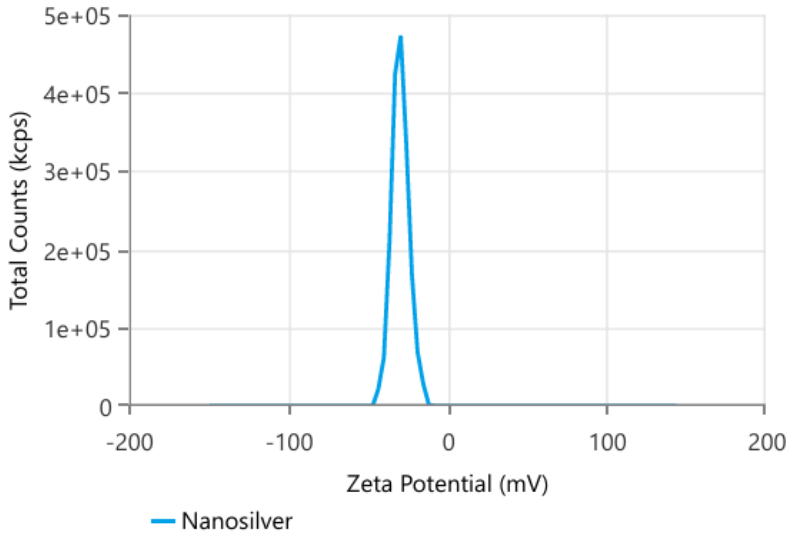


**Figure 4** Zeta potential distribution of AgNPs-AG, indicating the surface charge and colloidal stability of the biosynthesized silver nanoparticles in suspension.

***FTIR spectrum***

The FTIR spectrum shows shifts and changes in band intensity between *A. galanga* extract, $AgNO_3$ solution, and AgNPs-AG (**Figure 5**), indicating the involvement of extract biomolecules in the reduction and stabilization of nanoparticles [59]. The broad band around 3,317 $cm^{-1}$ represents the stretching vibration of –OH from phenolics and alcohols, consistent with the range of 3,391 - 3,468 [19] and 3,420 - 3,220 $cm^{-1}$ [60]. The shift and broadening of this band in silver nanoparticles confirms the role of the –OH group as an electron donor in the reduction of $Ag^+$ to $Ag^0$.

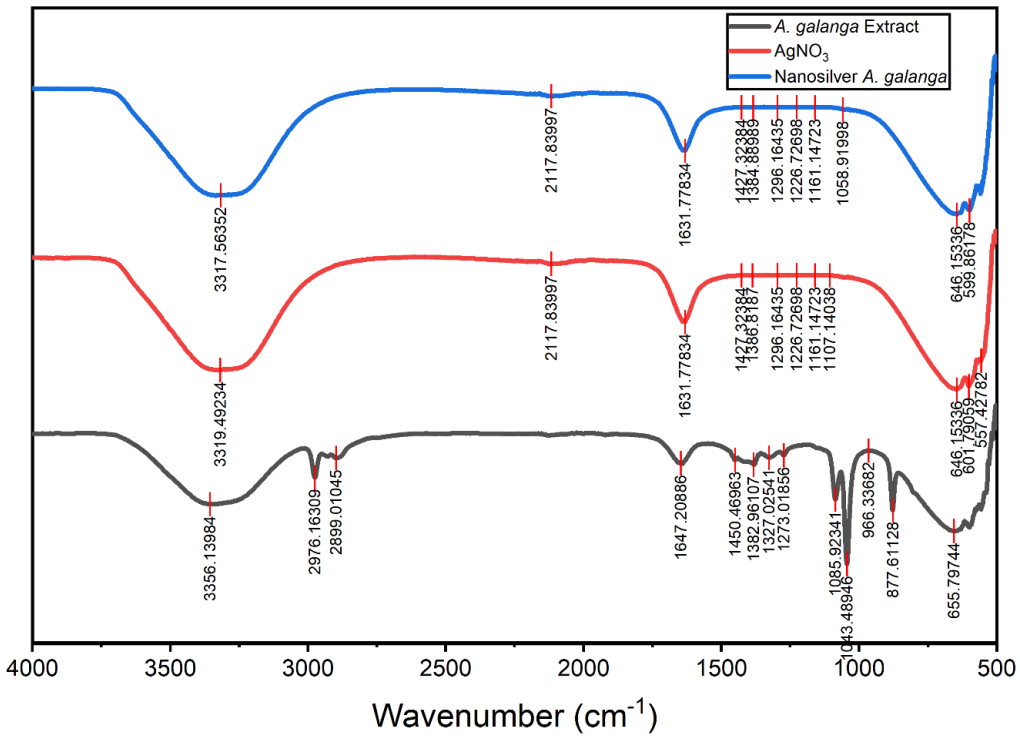


**Figure 5** FTIR spectra of *A. galanga* ethanol extract (black), $AgNO_3$ solution (red), and AgNPs-AG (blue), illustrating the functional groups involved in the reduction of $Ag^+$ ions and stabilization of the synthesized nanoparticles.

The 1,631 - 1,647 $cm^{-1}$ band is associated with C=O stretching vibrations of amides, flavonoids, and aromatic phenolics; bands in a similar range have also been reported to be associated with carboxylate and amide groups that play a role in the bioreduction of silver ions [49,60,61]. The 1,450 - 1,384 $cm^{-1}$ band indicates C–H and C–O vibrations from carboxylates and phenolics, as confirmed in studies by [19,62] and [63],which linked this band to carboxylate–$Ag^+$ interactions. The 1,296 - 1,226 $cm^{-1}$ range represents C–O–C and C–O alcohol/ether vibrations, similar to the FTIR profile of AgNPs biosynthesis using *Amorphophallus paeoniifolius* extract [64]. The disappearance of the strong band in the 1,085 - 877 $cm^{-1}$ region in silver nanoparticles urther reinforces the involvement of organic oxygen groups in the $Ag^+$ reduction process [19].

In addition, the band below 700 $cm^{-1}$ (646 - 599 $cm^{-1}$) indicates Ag–O and Ag–O–Ag vibrations, which signify the formation of metal-oxygen bonds in the AgNPs structure [59]. Overall, the FTIR profile confirms that the carbonyl, phenolic, amine, and polysaccharide groups in the *A. galanga* extract act as reducing agents and capping agents that stabilize the nanoparticles [60,63].

**Morphology of AgNPs-AG with SEM**

SEM micrographs at magnifications of 5,000× to 50,000× show that AgNPs-AG has a predominantly spherical morphology (**Figure 6**) with slight agglomeration forming small and relatively homogeneous aggregates [50]. This characteristic is consistent with other plant-based silver nanoparticles, such as *Cajanus cajan*, which has also been reported to

produce nearly spherical particles with minimal agglomeration [65]. In some areas, a thin layer is visible around the surface of the nanoparticles, which is thought to originate from the organic components of the *A. galanga* extract. This layer acts as a capping agent that coats the surface of AgNPs and serves to prevent excessive aggregation [66].

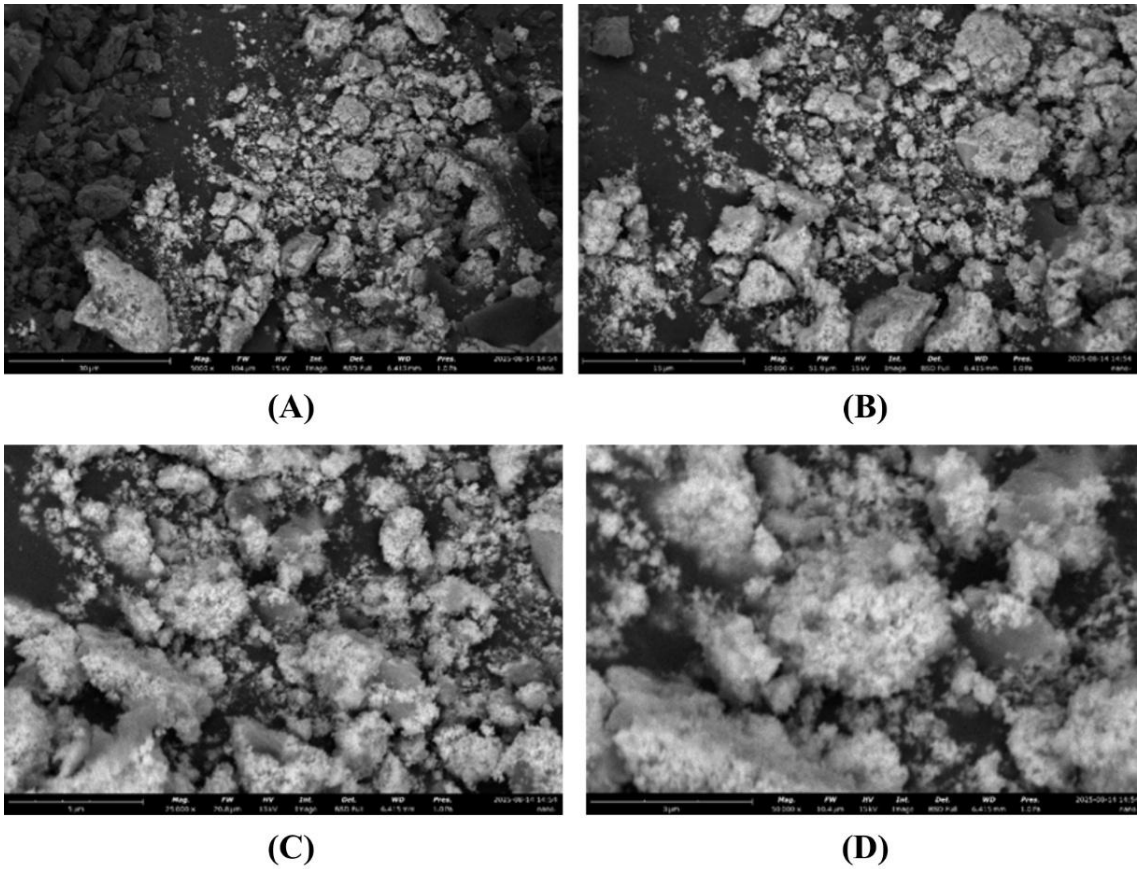


**Figure 6** SEM micrographs of silver nanoparticles synthesized using *A. galanga* extract (AgNPs-AG) at various magnifications: (A) 5,000×; (B) 10,000×; (C) 25,000×; (D) 50,000×, showing predominantly spherical morphology of AgNPs-AG.

**Cytotoxic activity of AgNPs-AG against Huh7it cells**

The cytotoxicity AgNPs-AG was assessed through the MTT assay at 24 and 48 h of exposure. The $IC_{50}$ value represents the concentration required to reduce cell viability by 50% and is widely used as a quantitative parameter to evaluate and compare the cytotoxic potency of anticancer candidates. $IC_{50}$ values derived from the concentration-response curves demonstrated a clear time-dependent reduction, where the $IC_{50}$ decreased from 71.046 µg/mL at 24 h to 63.395 µg/mL at 48 h (**Figure 7**), indicating increased cellular sensitivity during prolonged exposure. This pattern aligns with the time-dependent nature of cytotoxic responses described by Sánchez-Díez *et al.* [67] and the findings of Salispriaji *et al.* [68],which showed that $IC_{50}$ tends to decline as exposure duration increases. According to NCI criteria [69], these values fall within the moderately active cytotoxic category (21 - 200 µg/mL), indicating that AgNPs-AG possesses relevant inhibitory potential against Huh7it cells.

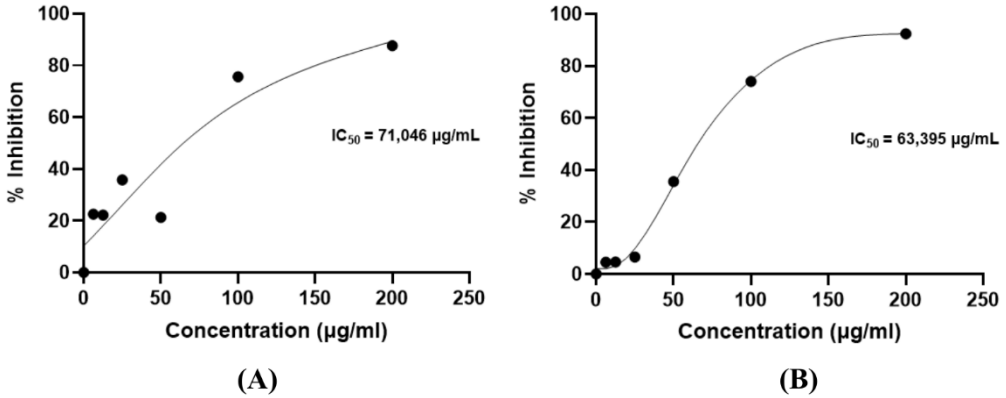


**Figure 7** Inhibition value ($IC_{50}$) of AgNPs-AG against Huh7it hepatocellular carcinoma cells after 24 (A) and 48 h (B) of exposure, determined by MTT assay.

Cell viability profiles supported these $IC_{50}$ findings (**Figure 8)**. At 24 h, lower concentrations (6.25 - 25 µg/mL) showed no significant reduction compared to the control, while notable decreases occurred at 100 and 200 µg/mL, which formed the lowest-viability groups. At 48 h, a more pronounced reduction was observed at concentrations ≥ 50 µg/mL, with 200 µg/mL producing the strongest inhibitory effect. Interestingly, at 24 h, the viability of DOX-treated cells was still comparable to low-dose AgNPs-AG, but at 48 h, the cytotoxic pattern of high-dose AgNPs-AG (≥ 100 µg/mL) began to approximate DOX activity, emphasizing the time-dependent cytotoxic enhancement. Overall, these findings demonstrate that the cytotoxic effect of AgNPs-AG on Huh7it cells is both dose-dependent and time-dependent.

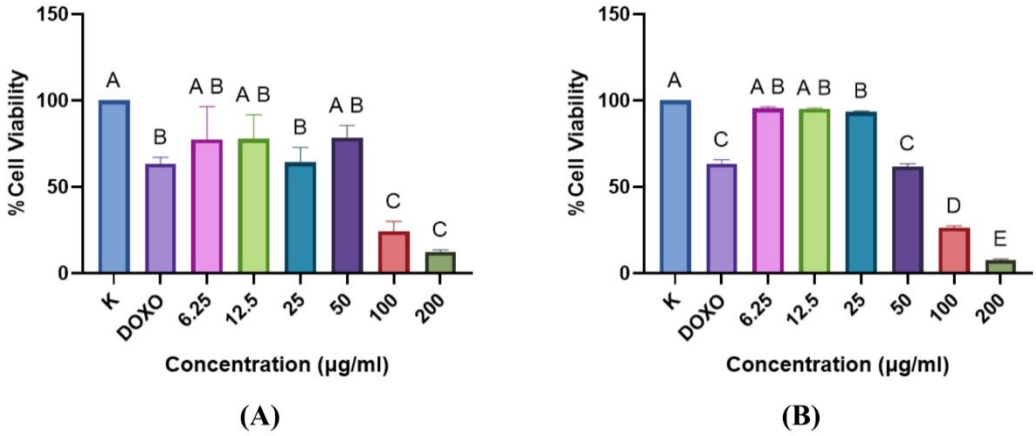


**Figure 8** Cell viability of Huh7it liver cancer cells after treatment with AgNPs-AG for 24 (A) and 48 h (B), assessed using the MTT assay. Data are presented as mean ± SD. Different letters indicate statistically significant differences between treatment groups ($p < 0.05$). DOX: doxorubicin.

The cytotoxic response is strongly influenced by the physical characteristics of the nanoparticles. SEM and PSA analyses revealed that AgNPs-AG exhibited predominantly spherical morphology with a size range of 6 - 20 nm, which enhances cellular interaction and internalization. Nanoparticles below 50 nm are known to penetrate cells via clathrin-mediated endocytosis and macropinocytosis [70,71], allowing accumulation in the cytoplasm and near mitochondria. Once internalized, AgNPs-AG releases $Ag^+$ ions that induce excessive ROS production, leading to oxidative damage of lipids, proteins, and nucleic acids [41]. Elevated ROS disrupts mitochondrial membrane potential and promotes cytochrome c release, activating caspase-9 and caspase-3, which are key executors of intrinsic apoptosis [72]. ROS can also activate JNK/p38-MAPK signaling,

enhancing Bax expression and suppressing Bcl-2, further promoting apoptosis [73]. These mechanisms are consistent with previous reports showing that AgNPs induce apoptosis, DNA damage, and cell-cycle arrest through p53 activation [74,75].

The intensified viability reduction at 48 h suggests progressive accumulation of apoptosis-related signals. Similar ROS-mediated apoptosis has been documented in AgNPs derived from *Cladosporium oxysporum* [76] and in studies showing caspase-3 activation in breast and lung cancer cells exposed to AgNPs [77]. Beyond apoptosis, AgNPs-AG may also inhibit proliferation through suppression of the PI3K/Akt/mTOR pathway, a central survival axis in cancer cells [78,79]. Reduced Akt phosphorylation by AgNPs-AG, along with decreased mTOR and Bcl-2 expression, reinforces pro-apoptotic signaling and limits proliferation [79,80], supporting earlier findings in HepG2 cells treated with AgNPs from *Catharanthus roseus* [81]. Although this study did not directly assess apoptotic markers or molecular signaling pathways, the observed cytotoxic patterns are strongly supported by extensive literature describing ROS-mediated apoptosis and cell cycle arrest induced by AgNPs.

The LC-MS profile of *A. galanga* provides additional mechanistic support for the cytotoxic activity of AgNPs-AG. Phenolic compounds such as hexahydrocurcumin (HHC) and cinnamaldehyde are known to enhance ROS generation, suppress PI3K/Akt and MAPK/ERK pathways, and activate apoptotic caspase-3/9 signaling [82-84]. Organic acids including DL-malic acid can induce intrinsic mitochondrial apoptosis via oxidative stress [85]. AgNPs-AG also displays a zeta potential of approximately –30 mV, contributing to colloidal stability and facilitating electrostatic interactions with the positively charged cancer cell membrane, promoting nanoparticle internalization and strengthening mitochondrial apoptotic signaling [84].

### *In silico* analysis

#### *Prediction of anticancer activity and pharmacokinetic properties*

PASS Online analysis is used to predict anticancer activity potential based on structure-activity relationships (SAR) [86]. PASS generates Pa and Pi values, and Pa > Pi indicates a higher possibility of biological activity [87]. The three compounds (**Table 2**) with the highest Pa values are 2,3-dihydroxybenzoylserine (Pa = 0.383), (9Z)-9-octadecenamide (Pa = 0.382), and citric acid (Pa = 0.352), all of which are in the Pa > 0.3 category, which is considered to have feasible anticancer potential [88].

**Table 2** Screening of potential anticancer activity of phytochemical compounds identified in the ethanol extract of *A. galanga* using LC-MS analysis.

| No. | Name | Compound ID (CID) | SMILES Cannonical | Anticancer Potential | |
|---|---|---|---|---|---|
| | | | | Pa | Pi |
| 1. | (9Z)-9-Octadecenamide | 5283387 | CCCCCCCC/C=C\CCCCCCCC(=O)N | 0.382 | 0.020 |
| 2. | 2,3-Dihydroxybenzoylserine | 151483 | C1=CC(=C(C(=C1)O)O)C(=O)N[C@@H](CO)C(=O)O | 0.383 | 0.020 |
| 3. | 2-C-methylerythritol 4-phosphate | 443198 | C[C@](CO)([C@@H](COP(=O)(O)O)O)O | 0.221 | 0.217 |
| 4. | 4-Aminobenzoic acid | 978 | C1=CC(=CC=C1C(=O)O)N | 0.335 | 0.053 |
| 5. | Alpha-Naphthoflavone | 11790 | C1=CC=C(C=C1)C2=CC(=O)C3=C(O2)C4=CC=CC=C4C=C3 | 0.311 | 0.082 |
| 6. | Choline | 305 | C[N+](C)(C)CCO | - | - |
| 7. | Cinnamaldehyde | 637511 | C1=CC=C(C=C1)/C=C/C=O | 0.343 | 0.046 |
| 8. | Citric acid | 311 | C(C(=O)O)C(CC(=O)O)(C(=O)O)O | 0.352 | 0.039 |
| 9. | D-(+)-galaktosa | 6036 | C([C@@H]1[C@@H]([C@@H]([C@H](C(O1)O)O)O)O)O | 0.319 | 0.015 |
| 10. | D-Glucono-δ-lactone | 7027 | C([C@@H]1[C@H]([C@@H]([C@H](C(=O)O1)O)O)O)O | 0.239 | 0.189 |
| 11. | Diacetin | 66021 | CC(=O)OCC(CO)OC(=O)C | 0.330 | 0.059 |

| No. | Name | Compound ID (CID) | SMILES Cannonical | Anticancer Potential | |
|---|---|---|---|---|---|
| | | | | Pa | Pi |
| 12. | DL-Malic acid | 525 | C(C(C(=O)O)O)C(=O)O | 0.361 | 0.032 |
| 13. | Guaitolin | 68825 | CCOC1=CC=CC=C1OCC(CO)O | 0.289 | 0.113 |
| 14. | Hexahidrocurcumin | 5318039 | COC1=C(C=CC(=C1)CCC(CC(=O)CCC2=CC(=C(C=C2)O)OC)O)O | 0.280 | 0.127 |
| 15. | L-(+)-valine | 6971018 | CC(C)[C@@H](C(=O)[O-])[NH3+] | 0.336 | 0.053 |
| 16. | N-Acetylneuraminic acid | 439197 | CC(=O)N[C@@H]1[C@H](CC(O[C@H]1[C@@H]([C@@H](CO)O)O)(C(=O)O)O)O | - | - |
| 17. | N-ethylmaleimide | 4362 | CCN1C(=O)C=CC1=O | 0.315 | 0.076 |
| 18. | N-Glycosyl-L-asparagine | 440002 | C([C@@H]1[C@H]([C@@H]([C@H]([C@@H](O1)NC(=O)C[C@@H](C(=O)O)N)O)O)O)O | 0.311 | 0.024 |
| 19. | Phenprocoumon | 54680692 | CCC(C1=CC=CC=C1)C2=C(C3=CC=CC=C3OC2=O)O | 0.289 | 0.113 |
| 20. | Piclamilast | 154575 | COC1=C(C=C(C=C1)C(=O)NC2=C(C=NC=C2Cl)Cl)OC3CCCC3 | 0.169 | 0.127 |

ADME evaluation using SwissADME and pkCSM showed that 2,3-dihydroxybenzoylserine, citric acid, and DL-malic acid met all parameters of Lipinski's Rule of Five, while (9Z)-9-octadecenamide did not pass due to a logP value > 5, indicating excessive lipophilicity [45,89]. Of the three, 2,3-dihydroxybenzoylserine has the most balanced profile (MW 241.20 Da, logP –0.73) with moderate polarity and good bioavailability [90,91]. Meanwhile, citric acid and malic acid are highly hydrophilic, resulting in lower membrane permeability [92]. Therefore, 2,3-dihydroxybenzoylserine emerges as the most promising candidate for further molecular docking studies.

**Molecular docking**

Molecular docking was performed against four key liver cancer proteins, namely p53, caspase-9, EGFR, and CDK4, using doxorubicin as a comparative control [93]. A more negative binding affinity indicates a more stable complex (**Table 3** and **Figure 9**). The results show that 2,3-dihydroxybenzoylserine has the strongest affinity compared to other compounds, with values of –6.1 kcal/mol (p53), –7.3 kcal/mol (caspase-9), –6.6 kcal/mol (EGFR), and –5.9 kcal/mol (CDK4), approaching the stability of doxorubicin (–8.2 to –9.6 kcal/mol). These *in silico* results provide a molecular rationale for the anticancer activity observed *in vitro*. The strong and stable interactions of 2,3-dihydroxybenzoylserine with key regulatory proteins involved in apoptosis and cell proliferation suggest that the cytotoxic effects of AgNP–AG on Huh7it cells may be mediated through modulation of multiple cancer-related signaling pathways. In particular, the predicted binding to p53 and caspase-9 supports the induction of intrinsic apoptosis, while interactions with EGFR and CDK4 indicate potential suppression of proliferative signaling and cell cycle progression, consistent with the *in vitro* antiproliferative effects.

In p53, interactions via hydrogen bonds with Thr211, Gly199, and Leu201, as well as hydrophobic interactions with Leu188 and Val172, indicate stabilization of the p53 conformation, a mechanism that is also commonly observed in control ligands [94]. In caspase-9, binding to Arg178, a critical residue at the active site [17], reinforces the possibility of intrinsic apoptosis pathway activation.

Interactions with EGFR show similarity in binding residues with doxorubicin, which according to Dwijayanti *et al.* [93] indicates potential inhibition of the PI3K/Akt pathway, a dominant pathway in HCC progression. In CDK4, binding to Asp126 and His65, as well as hydrophobic interactions with Phe127, indicate potential inhibition of the CDK4/Cyclin D1 complex, which has implications for cell cycle arrest [95].

**Table 3** Molecular docking results showing the interactions between selected ligands and cancer-related target proteins, including p53, caspase-9, EGFR, and CDK4.

| Protein | Compound | Bond Affinity (kcal/mol) | Types of bonds | | |
|---|---|---|---|---|---|
| | | | Hydrogen | Hydrophobic | Van Der Waals |
| **p53** | Doxorubicin (Control) | −8.7 | Glu171 | Val172, Cys139, His168 | Thr123, Gln167, Arg174, Glu198, Gly199 |
| | (9Z)-9-Octadecenamide | −4.8 | **Gly199** | Val97, His233, Ile232, Val218 | Ser96, Glu224, Pro222, Thr231, Asn200, Thr230, Glu221, Pro219 |
| | **2,3-Dihydroxy benzoylserine** | −6.1 | Thr211, **Gly199**, Leu201 | Leu188 | Phe212, **Val172**, Arg213, Ser96, Thr170, Asn210, **Glu198**, Val203 |
| | Citric acid | −5.3 | **His168**, **Gln167**, **Glu198**, Ala138, **Cys139** | - | **Val172**, **Glu171**, Met169, Asn235, Arg196 |
| | DL-Malic acid | −5.6 | Thr170, **Glu171**, Ala138, Thr140 | - | **His168**, Gln167, Arg249, **Glu198**, **Cys139**, Asn235 |
| **Caspase 9** | Doxorubicin (Control) | −9.2 | Asp186, Ser287, Gln285, Arg180, Thr181 | Lys358, Pro357, Phe351, Arg178 | Thr179, Gly182, Ser183, His237, Gly288, Phe348, Pro349, Gly350, Ser361 |
| | (9Z)-9-Octadecenamide | −4.4 | Lys410, Ser382 | Leu151, Leu145, Trp374, Ile396 | Asn148, Ser144, Arg386, Glu378, Ser377, Tyr397 |
| | **2,3-Dihydroxybenzoylserine** | −7.3 | **Pro357**, **Thr179**, **Ser361** | Arg178 | **Asp186**, **Phe351**, **His237**, Ala286, **Gln285**, **Ser287**, **Phe348**, **Pro349**, **Ser183**, **Gly350**, Lys358, **Gly182** |
| | Citric acid | −6.1 | **Arg180**, **Ser287**, **Thr181** | - | **Asp186**, **Gly182**, Gly360, **Ser361**, **Gln285**, Ala286, **His237**, **Ser183**, **Phe351** |
| | DL-Malic acid | −5.2 | **Asp186**, **Arg180**, **Gln285**, **Pro357**, **Ser287** | - | Gly360, **Phe351**, **Ser361**, **Pro349**, **Phe348**, **Ser183**, **Gly182**, **Thr181**, **Lys358** |
| **EGFR** | Doxorubicin (Control) | −9.6 | Ser196, Gln194, His209 | Cys207, His209 | Asn210, Gln194, Cys195, Cys208, Cys207, Gly197, Arg220, Cys195, Pro219, Glu221 |
| | (9Z)-9-Octadecenamide | −5.1 | Ser342, Thr378 | Phe380, Ile318, His409, Tyr44, Ile38 | His346, Gln408, Lys407, Asp344, Thr406, Arg285, Gly343, Gly379, Arg405 |
| | **2,3-Dihydroxybenzoylserine** | −6.6 | **Ser196**, **Cys208** | **Cys207** | Ser205, Pro204, **Gln194**, **Pro219**, **His209**, **Asn210**, **Cys207**, Pro204, Ser205, **Pro219**, **Gly197**, **Gln194**, **Cys195** |
| | Citric acid | −5.4 | Glu60, Arg84, Ala265, Arg231, Cys227 | - | Val36, Val226, Lys229, Leu225, Phe230 |
| | DL-Malic acid | −4.5 | Tyr246, Met244, Ser262, Gly281, Lys260 | - | Pro242, Met253, Leu245, His280, Thr239, Ser282, Pro242, Cys240, Tyr261 |
| **CDK4** | Doxorubicin (Control) | −8.2 | Leu148, Asn151, Arg58, Ala62, Lys33, Thr37 | Arg87, Leu91 | Ser90, Pro40, Ser41, Ala39, Ala34, Lys149, Glu36, Glu64, Glu61 |
| | (9Z)-9-Octadecenamide | −5.2 | Arg123, Leu287 | Ala30, Ala130, Phe63, Phe127, His65 | Arg26, Phe284, Asp126, Asn131 |
| | **2,3-Dihydroxybenzoylserine** | −5.9 | Asp126, His65, Arg123 | Ala30, Ala130, Phe127, Phe63 | Leu287, Phe284, Asn131 |
| | Citric acid | −4.9 | Arg218, Val212, Asn222, Asn221 | - | Ile178, Gln213, Pro220, Asn174, Ser219, Leu217, His181, Ile177, Gly214, Ala211 |
| | DL-Malic acid | −4.7 | Asn146, Lys149, Val74, Asp73 | - | Trp150, Lys147, Cys75, Ala76, Met52, Ser56 |

Amino acids: Amino acid residues that share similarities with the interactions between the control compound and the protein

The selection of test receptors in the form of EGFR, p53, caspase-9, and CDK-4 proteins was based on the function of each receptor, which is important for the regulation of cancer. The EGFR protein is one of the main oncogenes causing hepatocellular carcinoma. Increased EGFR activation will result in increased proliferation and resistance to apoptosis through the PI3K/Akt/mTOR pathway. EGFR inhibition can reduce liver cancer cell growth and increase the effects of anticancer drugs [96]. The p53 protein plays an important role in regulating the cell cycle and apoptosis. Mutations in the form of p53 inactivation in cells, which occur in most cases of HCC, contribute to tumor growth and drug resistance [97]. Caspase-9 plays a role as a key enzyme in the intrinsic apoptosis pathway activated by the release of cytochrome-c from the mitochondria. Activation of caspase-9 triggers a caspase cascade that causes programmed cell death, making it an important target in pro-apoptotic strategies for liver cancer [98]. CDK-4 plays a role in the G1-S phase transition in the cell cycle and is often overexpressed in hepatocellular carcinoma. Inhibition of CDK4 can cause cell cycle arrest and suppress tumor growth [99].

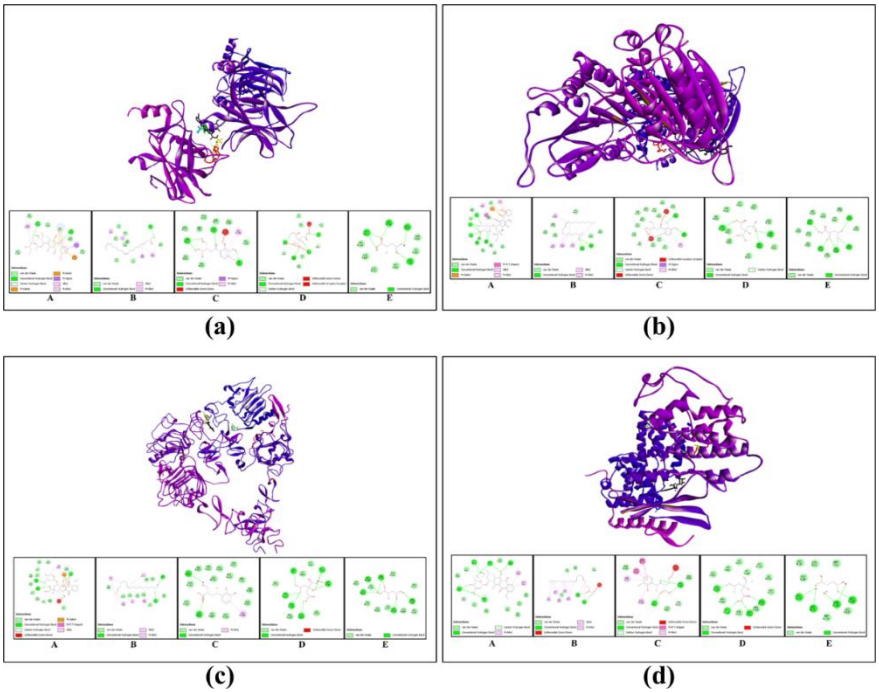


**Figure 9** Molecular docking interactions of selected ligands with cancer-related protein targets. Three-dimensional docking poses (upper panels) and 2-dimensional interaction maps (lower panels) illustrate the binding interactions between bioactive compounds from *Alpinia galanga* extract and key regulatory proteins. (a) p53, (b) Caspase-9, (c) EGFR, and (d) CDK4. For each protein, the docked ligands are (A) doxorubicin (reference drug), (B) (9Z)-9-octadecenamide, (C) 2,3-dihydroxybenzoylserine, (D) citric acid, and (E) DL-malic acid.

These docking findings are consistent with *in vitro* results, namely a decrease in viability at high doses and 48-hour exposure, pointing to a mechanism involving oxidative stress, p53-caspase-9 activation, and proliferation inhibition. Therefore, 2,3-dihydroxybenzoylserine emerges as the primary metabolite candidate contributing to the cytotoxic effects of AgNPs-AG, while also reinforcing the potential of these nanoparticles for therapeutic development in HCC.

**Conclusions**

This study revealed that ethanol extract from *Alpinia galanga* rhizome is a promising biomaterial for the synthesis of green silver nanoparticles and has significant anticancer potential against hepatocellular carcinoma. LC-MS profiling identified 20 metabolites, with 2,3-dihydroxybenzoic acid as the dominant

compound, possibly contributing to nanoparticle reduction and stabilization as well as anticancer activity. The synthesized silver nanoparticles (AgNPs) exhibited favorable physicochemical characteristics, including a characteristic SPR peak at 420 nm, functional groups (–OH and C=O), small and uniform particle size (average 6.35 nm), and a zeta potential of approximately −30 mV, indicating good colloidal stability. Biologically, AgNPs-AG reduced Huh7it cell viability in a dose- and time-dependent manner, leading to moderate $IC_{50}$ values at 24 and 48 h. Supporting these findings, *in silico* analysis demonstrated strong binding affinity of 2,3-dihydroxybenzoic acid to caspase-9 and stable interactions with EGFR, CDK4, and p53, suggesting potential mechanisms of apoptosis induction and cell proliferation inhibition. Despite these encouraging results, this study is limited to *in vitro* cytotoxicity evaluation and computational predictions, without direct mechanistic or *in vivo* validation. Future studies should focus on tracing the molecular pathways underlying the anticancer effects, evaluating selectivity toward cancer cells versus normal cells, and assessing *in vivo* efficacy and safety to further support the therapeutic potential of the silver nanoparticles system derived from *A. galanga*.

**Acknowledgements**

The authors would like to thank the Faculty of Science and Technology, Airlangga University, Indonesia and the Master's Degree Scholarship for Outstanding Undergraduates (PMDSU) provided by the Indonesian Ministry of Research, Technology, and Higher Education for their support. Research and higher education activities are funded by the Indonesian Ministry of Research and Higher Education [PMDSU 2025 (NKI:059/C3/DT.05.00/PL/2025) and (NKT:2414/B/UN3LPPM/PT.01.03/2025)].

**Declaration of generative AI in scientific writing**

The authors acknowledge the use of generative AI tools (e.g., QuillBot and ChatGPT by OpenAI) in the preparation of this manuscript, specifically for language editing and grammar correction. No content generation or data interpretation was performed by AI. The authors take full responsibility for the content and conclusions of this work.

**CRediT author statement**

**Rr Aulia Rahmawati Kusuma Putri**: Conceptualization; Methodology; Data curation; Writing - Original Draft. **Mochammad Aqilah Herdiansyah**: Methodology; Formal analysis; Software; Visualization. **Aulia Umi Rohmatika**: Investigation; Resources; Data curation; Writing - Review & Editing. **Sri Rahayu**: Validation; Investigation; Writing - Review & Editing. **Win Darmanto**: Supervision; Investigation; Project administration; Funding acquisition; Writing - Review & Editing.

**References**

[1] H Sung, J Ferlay, RL Siegel, M Laversanne, I Soerjomataram, A Jemal and F Bray. Global cancer statistics 2020: GLOBOCAN estimates of incidence and mortality worldwide for 36 cancers in 185 countries. *CA: A Cancer Journal for Clinicians* 2021; **71(3)**, 209-249.

[2] A Alqahtani, Z Khan, A Alloghbi, TS Said Ahmed, M Ashraf and DM Hammouda. Hepatocellular carcinoma: Molecular mechanisms and targeted therapies. *Medicina* 2019; **55(9)**, 526.

[3] J Wang, K Qiu, S Zhou, Y Gan, K Jiang, D Wang and H Wang. Risk factors for hepatocellular carcinoma: An umbrella review of systematic review and meta-analysis. *Annals of Medicine* 2025; **57(1)**, 2455539.

[4] M Dimri and A Satyanarayana. Molecular signaling pathways and therapeutic targets in hepatocellular carcinoma. *Cancers* 2020; **12(2)**, 491.

[5] YH Su, KF Ng, MC Yu, TJ Wu, TS Yeh, WC Lee, YS Lin, TH Hsieh, CY Lin, CT Yeh and TC Chen. Impact of epidermal growth factor receptor protein and gene alteration on Taiwanese hepatocellular carcinomas. *Journal of Gastroenterology and Hepatology* 2015; **30(9)**, 1397-1404.

[6] Z Li, L Qu, W Luo, Y Tian, H Zhai, K Xu and H Zhong. Mig-6 is down-regulated in HCC and inhibits the proliferation of HCC cells via the P-ERK/Cyclin D1 pathway. *Experimental and Molecular Pathology* 2017; **102(3)**, 492-499.

[7] D Wang, W Ruan, L Fan, H Xu, Q Song, H Diao, R He, Y Jin and A Zhang. Hypermethylation of *Mig-6* gene promoter region inactivates its

function, leading to EGFR/ERK signaling hyperphosphorylation, and is involved in arsenite-induced hepatic stellate cells activation and extracellular matrix deposition. *Journal of Hazardous Materials* 2022; **439**, 129577.

[8] S Gao, X Jiang, L Wang, S Jiang, H Luo, Y Chen and C Peng. The pathogenesis of liver cancer and the therapeutic potential of bioactive substances. *Frontiers in Pharmacology* 2022; **13**, 1029601.

[9] R Kim, T Kin and WT Beck. Impact of complex apoptotic signaling pathways on cancer cell sensitivity to therapy. *Cancers* 2024; **16(5)**, 984.

[10] AR Khairullah, TI Solikhah, ANM Ansori, A Fadholly, SC Ramandinianto, R Ansharieta, A Widodo, KHP Riwu, N Putri, A Proboningrat, MKJ Kusala, BW Rendragraha, ARS Putra and A Anshori. A review of an important medicinal plant: *Alpinia galanga* (L.) Willd. *Systematic Reviews in Pharmacy* 2020; **11(10)**, 387-395.

[11] K Mardhiyyah, YI Ryandini and Y Hermawan. Red and white galangal puree antioxidant activity and phytochemistry screening. *Jurnal Jamu Indonesia* 2021; **6(1)**, 23-31.

[12] J Li, JYS Lim, JQ Eu, AKMH Chan, BC Goh, L Wang and ALA Wong. Reactive oxygen species modulation in the current landscape of anticancer therapies. *Antioxidants & Redox Signaling* 2024; **41(4-6)**, 322-341.

[13] RG Baradwaj, MV Rao and TS Kumar. Novel purification of 1'S-1'-acetoxychavicol acetate from *Alpinia galanga* and its cytotoxic plus antiproliferative activity in colorectal adenocarcinoma cell line SW480. *Biomedicine & Pharmacotherapy* 2017; **91**, 485-493.

[14] MJ Nirmala, U Kizhuveetil, A Johnson, R Nagarajan and V Muthuvijayan. Cancer nanomedicine: A review of nano-therapeutics and challenges ahead. *RSC Advances* 2023; **13(13)**, 8606-8629.

[15] H Atmaca, ÇÇ Pulat and S Ilhan. Synthesis of silver nanoparticles using *Alpinia officinarum* rhizome extract induces apoptosis through down-regulating Bcl-2 in human cancer cells. *Biologia Futura* 2022; **73(3)**, 327-334.

[16] G Mustafa, S Younas, HS Mahrosh, MF Albeshr and EA Bhat. Molecular docking and simulation-binding analysis of plant phytochemicals with the hepatocellular carcinoma targets epidermal growth factor receptor and caspase-9. *Molecules* 2023; **28(8)**, 3583.

[17] Y Saubari, K Nastiti dan M Mambang. Uji farmakognostik and identidikasi senyawa pada beberapa tingkatan fraksi ekstrak etanol daun lengkuas (*Alpinia galanga*) (*in Indonesian*). *Journal Pharmaceutical Care and Sciences* 2020; **1(1)**, 102-110.

[18] MI Tangkau, Fatimawali and EJ Suoth. Antioxidant activity of ethanol extract white Galangal stem (*Alpina galanga*) with ABTS method. *Pharmacon* 2023; **12(3)**, 358-366.

[19] E Ahmad, A Athar, Nimisha, Q Zia, AK Sharma, M Sajid, M Bharadwaj, MA Ansari and SS Saluja. Harnessing nature's potential: *Alpinia galanga* methanolic extract mediated green synthesis of silver nanoparticle, characterization and evaluation of anti-neoplastic activity. *Bioprocess and Biosystems Engineering* 2024; **47(8)**, 1183-1196.

[20] RB Patil and AD Chougale. Analytical methods for the identification and characterization of silver nanoparticles: A brief review. *Materials Today: Proceedings* 2021; **47**, 5520-5532.

[21] AA Azmi and NM Ahyat. Green synthesis of silver nanoparticles using rhizhome extract of galangal, *Alpinia galanga*. *Malaysian Journal of Analytical Sciences* 2015; **19(6)**, 1187-1193.

[22] G Rajkumar and R Sundar. Biogenic one-step synthesis of silver nanoparticles (AgNPs) using an aqueous extract of *Persea americana* seed: Characterization, phytochemical screening, antibacterial, antifungal and antioxidant activities. *Inorganic Chemistry Communications* 2022; **143**, 109817.

[23] S Hayaza, SPA Wahyuningsih, RJK Susilo, AA Permanasari, SA Husen, D Winarni, H Punnapayak and W Darmanto. Anticancer activity of okra raw polysaccharides extracts against human liver cancer cells. *Tropical Journal of Pharmaceutical Research* 2019; **18(8)**, 1667-1672.

[24] MA Herdiansyah, ANM Ansori, VD Kharisma, MRT Alifiansyah, D Anggraini, QAP Priyono, PA Yusniasari, AJT Fetty, R Zainul, M Rebezov, E Kolesnik and N Maksimiuk. *In silico* study of

cladosporol and its acyl derivatives as anti-breast cancer against alpha-estrogen receptor. *Biosaintifika: Journal of Biology & Biology Education* 2024; **16(1)**, 142-154.

[25] NS Aini, ANM Ansori, MA Herdiansyah, VD Kharisma, MH Widyananda, AAA Murtadlo and H Purnobasuki. Antimalarial potential of phytochemical compounds from *Garcinia atroviridis* Griff. ex T. Anders targeting multiple proteins of *Plasmodium falciparum* 3D7: An in silico approach. *BIO Integration* 2024; **5(1),** 967.

[26] SH Deshpande, AB Muhsinah, ZK Bagewadi, GM Ankad, MH Mahnashi, DA Yaraguppi, IA Shaikh, AA Khan, HV Hegde and S Roy. In silico study on the interactions, molecular docking, dynamics and simulation of potential compounds from *Withania somnifera* (L.) Dunal root against cancer by targeting KAT6A. *Molecules* 2023; **28(3),** 1117.

[27] G Suresh Kumar, R Manivannan and B Nivetha. *In silico* identification of flavonoids from *Corriandrum sativum* seeds against Coronavirus Covid-19 main protease. *Journal of Drug Delivery & Therapeutics* 2021; **11(2)**, 145-152.

[28] L Marciniak, M Nowak, A Trojanowska, B Tylkowski and R Jastrzab. The effect of pH on the size of silver nanoparticles obtained in the reduction reaction with citric and malic acids. *Materials* 2020; **13(23)**, 5444.

[29] M Kamali, SAA Ghorashi and MA Asadollahi. Controllable synthesis of silver nanoparticles using citrate as complexing agent: Characterization of nanopartciles and effect of pH on size and crystallinity. *Iranian Journal of Chemistry and Chemical Engineering* 2012; **31(4)**, 21-28.

[30] D Veeragoni, S Deshpande, HK Rachamalla, A Ande, S Misra and SR Mutheneni. *In vitro* and *in vivo* anticancer and genotoxicity profiles of green synthesized and chemically synthesized silver nanoparticles. *ACS Applied Bio Materials* 2022; **5(5)**, 2324-2339.

[31] SY Wang, H Zhao, HT Xu, XD Han, YS Wu, FF Xu, XB Yang, U Göransson and B Liu. *Kaempferia galanga* L.: Progresses in phytochemistry, pharmacology, toxicology and ethnomedicinal uses. *Frontiers in Pharmacology* 2021; **12**, 675350.

[32] T Ziruo, M Shulipan, WY Zhang and WT Zhou. Cinnamaldehyde induces apoptosis of human cervical cancer SiHa cells and down-regulates the expression of HPV E6/E7 protein. *Natural Product Research and Development* 2022; **34(9)**, 1565-1572.

[33] A Abbassi, P Yaghmaei and L Hosseinzadeh. Cinnamaldehyde potentiates cytotoxic and apoptogenic effects of doxorubicin in prostate cancer cell line. *Research in Pharmaceutical Sciences* 2024; **19(4)**, 425-435.

[34] W An, Y Zhang, H Lai, Y Zhang, H Zhang, G Zhao, M Liu, Y Li, X Lin and S Cao. *Alpinia katsumadai* Hayata induces growth inhibition and autophagy-related apoptosis by regulating the AMPK and Akt/mTOR/p70S6K signaling pathways in cancer cells. *Oncology Reports* 2022; **48(2)**, 142.

[35] J Fu, Y Wang, M Sun, Y Xu and L Chen. Antibacterial activity and components of the methanol-phase extract from rhizomes of pharmacophagous plant *Alpinia officinarum* Hance. *Molecules* 2022; **27(13)**, 4308.

[36] N Maiti, VV Malkar, T Mukherjee and S Kapoor. Investigating the interaction of aminopolycarboxylic acid (APCA) ligands with silver nanoparticles: A Raman, surface-enhanced Raman and density functional theoretical study. *Journal of Molecular Structure* 2018; **1156**, 592-601.

[37] S Jayant, JJ Khandare, Y Wang, AP Singh, N Vorsa and T Minko. Targeted sialic acid–doxorubicin prodrugs for intracellular delivery and cancer treatment. *Pharmaceutical Research* 2007; **24(11)**, 2120-2130.

[38] A Vatankhah, SH Moghaddam, F Oroojalian, P Kesharwani and A Sahebkar. Sialic acid-functionalized nanomaterials for targeted cancer therapy, diagnosis, and theranostics. *International Journal of Pharmaceutics* 2025; **681**, 125901.

[39] C Battisegola, C Billi, MC Molaro, ME Schiano, M Nieddu, M Failla, E Marini, S Albrizio, F Sodano and MG Rimoli. Galactose: A versatile vector unveiling the potentials in drug delivery, diagnostics, and theranostics. *Pharmaceuticals* 2024; **17(3)**, 308.

[40] A Corti, AM Gasparri, M Ghitti, A Sacchi, F Sudati, M Fiocchi, V Buttiglione, L Perani, A Gori, S Valtorta, RM Moresco, F Pastorino, M Ponzoni, G Musco and F Curnis. Glycine N-methylation in NGR-tagged nanocarriers prevents isoaspartate formation and integrin binding without impairing CD13 recognition and tumor homing. *Advanced Functional Materials* 2017; **27(36)**, 1701245.

[41] L Boek-Dohalská, P Hodek, M Šulc and M Stiborová. α-Naphthoflavone acts as activator and reversible or irreversible inhibitor of rabbit microsomal CYP3A6. *Chemico-Biological Interactions* 2001; **138(1)**, 85-106.

[42] D Zhou, D Chen, J Wu, T Feng, P Liu and J Xu. Dicerandrol C suppresses proliferation and induces apoptosis of HepG2 and HeLa cancer cells by inhibiting β-catenin signaling pathway. *Marine Drugs* 2022; **22(6)**, 278.

[43] OL Nosareva, DS Orlov, EV Shakhristova and EA Stepovaya. Molecular mechanisms of the effects of *n*-ethylmaleimide and 1,4-dithioerythritol on regulation of apoptosis in P19 cells under hypoxia. *Bulletin of Siberian Medicine* 2020; **19(2)**, 72-77.

[44] Q Zheng, H Yang, J Wei, JL Tong and YQ Shu. The role and mechanisms of nanoparticles to enhance radiosensitivity in hepatocellular cell. *Biomedicine & Pharmacotherapy* 2013; **67(7)**, 569-575.

[45] X Chen, H Li, L Tian, Q Li, J Luo and Y Zhang. Analysis of the physicochemical properties of acaricides based on Lipinski's rule of five. *Journal of Computational Biology* 2020; **27(9)**, 1397-1406.

[46] NI Mongalo, OS Soyingbe and TJ Makhafola. Antimicrobial, cytotoxicity, anticancer and antioxidant activities of *Jatropha zeyheri* Sond. roots (Euphorbiaceae). *Asian Pacific Journal of Tropical Biomedicine* 2019; **9(7)**, 307-314.

[47] X Chen, H Li, L Tian, Q Li, J Luo and Y Zhang. Analysis of the physicochemical properties of acaricides based on Lipinski's rule of five. *Journal of Computational Biology* 2022; **27(9)**, 1397-1406.

[48] Y Haryani, Y Melanie, M Novita, R Hendra and GF Kartika. IAI SPECIAL EDITION: Green synthesis of silver nanoparticles from *Alpinia galanga* extract with microwave irradiation and antibacterial activity against *Escherichia coli*. *Pharmacy Education* 2022; **22(2)**, 20-23.

[49] P Imchen, M Ziekhrü, BK Zhimomi and T Phucho. Biosynthesis of silver nanoparticles using the extract of *Alpinia galanga* rhizome and *Rhus semialata* fruit and their antibacterial activity. *Inorganic Chemistry Communications* 2022; **142**, 109599.

[50] M Asif, R Yasmin, R Asif, A Ambreen, M Mustafa and S Umbreen. Green synthesis of silver nanoparticles (AgNPs), structural characterization, and their antibacterial potential. *Dose-Response* 2022; **20(2)**, 15593258221088709.

[51] AH Watoni, LOAN Ramadhan, MD Rahmatullah, AIDK Bunga and Supardi. Optimization of silver nanoparticles synthesis using *Alpinia galanga* L. Willd rhizome extract and their stability study. *Journal of Pure & Applied Chemistry Research* 2022; **11(1)**, 83-101.

[52] MA Sofi, S Sunitha, SK Pasha and D Choi. An overview of antimicrobial and anticancer potential of silver nanoparticles. *Journal of King Saud University - Science* 2022; **34(2)**, 101791.

[53] F Rodríguez-Félix, AG López-Cota, MJ Moreno-Vásquez, AZ Graciano-Verdugo, IE Quintero-Reyes, CL Del-Toro-Sánchez and JA Tapia-Hernández. Sustainable-green synthesis of silver nanoparticles using safflower (*Carthamus tinctorius* L.) waste extract and its antibacterial activity. *Heliyon* 2021; **7(4)**, e06923.

[54] S Hemmati, A Rashtiani, MM Zangeneh, P Mohammadi, A Zangeneh and H Veisi. Green synthesis and characterization of silver nanoparticles using *Fritillaria* flower extract and their antibacterial activity against some human pathogens. *Polyhedron* 2019; **158**, 8-14.

[55] A Almatroudi. Unlocking the potential of silver nanoparticles: From synthesis to versatile bio-applications. *Pharmaceutics* 2024; **16(9)**, 1232.

[56] AK Alzubaidi, WJ Al-Kaabi, A Al Ali, S Albukhaty, H Al-Karagoly, GM Sulaiman, M Asiri and Y Khane. Green synthesis and characterization of silver nanoparticles using flaxseed extract and evaluation of their antibacterial and antioxidant activities. *Applied*

*Sciences* 2023; **13(4)**, 2182.

[57] P Khandel, SK Shahi, DK Soni, RK Yadaw and L Kanwar. *Alpinia calcarata*: potential source for the fabrication of bioactive silver nanoparticles. *Nano Convergence* 2018; **5(1)**, 37.

[58] S Behboodi, F Baghbani-Arani, S Abdalan and SA Sadat Shandiz. Green engineered biomolecule-capped silver nanoparticles fabricated from *Cichorium intybus* extract: *In vitro* assessment on apoptosis properties toward human breast cancer (MCF-7) cells. *Biological Trace Element Research* 2019; **187(2)**, 392-402.

[59] S Pasieczna-Patkowska, M Cichy and J Flieger. Application of Fourier transform infrared (FTIR) spectroscopy in characterization of green synthesized nanoparticles. *Molecules* 2025; **30(3)**, 684.

[60] S Joseph and B Mathew. Microwave assisted biosynthesis of silver nanoparticles using the rhizome extract of *Alpinia galanga* and evaluation of their catalytic and antimicrobial activities. *Journal of Nanoparticles* 2014; **2014(1)**, 967802.

[61] S Perugu, V Nagati and M Bhanoori. Green synthesis of silver nanoparticles using leaf extract of medicinally potent plant *Saraca indica*: a novel study. *Applied Nanoscience* 2016; **6(5)**, 747-753.

[62] A Salayová, Z Bedlovičová, N Daneu, M Baláž, Z Lukáčová Bujňáková, Ľ Balážová and Ľ Tkáčiková. Green synthesis of silver nanoparticles with antibacterial activity using various medicinal plant extracts: Morphology and antibacterial efficacy. *Nanomaterials* 2021; **11(4)**, 1005.

[63] SEI Boudagha, C Sobhi, H Bendif, EÖÇ Uyanikgil, A Abdennouri, M Ökeer, C Bensouici, M Boudiaf, A Zouaoui, HA Rudayni, F Boufahja and S Garzoli. Green synthesis of silver nanoparticles using *Cynoglossum creticum* leaf extract: eco-friendly approach for antibacterial, antioxidant, and sensing applications. *Appl. Biochem. Biotechnol.* 2025; **197(12)**, 7981-8007.

[64] SM Abu Nayem, N Sultana, MA Haque, B Miah, MM Hasan, T Islam, MM Hasan, A Awal, J Uddin and AJS Ahammad. Green synthesis of gold and silver nanoparticles by using *Amorphophallus paeoniifolius* tuber extract and evaluation of their antibacterial activity. *Molecules* 2020; **25(20)**, 4773.

[65] V Babu Nagati, R Koyyati, MR Donda, J Alwala, KR Kundle and PRM Padigya. Green synthesis and characterization of silver nanoparticles from *Cajanus cajan* leaf extract and its antibacterial activity. *International Journal of Nanomaterials and Biostructures* 2012; **2(3)**, 39-43.

[66] F Esmaile, H Koohestani and H Abdollah-Pour. Characterization and antibacterial activity of silver nanoparticles green synthesized using *Ziziphora clinopodioides* extract. *Environmental Nanotechnology, Monitoring & Management* 2020; **14**, 100303.

[67] M Sánchez-Díez, P Romero-Jiménez, N Alegría-Aravena, CE Gavira-O'Neill, E Vicente-García, J Quiroz-Troncoso, R González-Martos, C Ramírez-Castillejo and JM Pastor. Assessment of cell viability in drug therapy: $IC_{50}$ and other new time-independent indices for evaluating chemotherapy efficacy. *Pharmaceutics* 2025; **17(2)**, 247.

[68] S Salispriaji, APD Nurhayati, M Santoso and FA Wati. Effect of Trisindolina-5 compound on Cancer Stem Cell (CSC) proliferation *in-vitro*. *BIO Web of Conferences* 2024; **89**, 01005.

[69] RI Geran, NH Greenberg, MM MacDonald. Protocols for screening chemical agents and natural products against animal tumors and other biological systems. *Cancer Chemotherapy Reports* 1972; **3(2)**, 17-27.

[70] SF Thai, KA Wallace, CP Jones, H Ren, BT Castellon, J Crooks, EA Grulke and KT Kitchin. Differential genomic effects on signaling pathways by two different $CeO_2$ nanoparticles in HepG2 cells. *Journal of Nanoscience and Nanotechnology* 2015; **15(12)**, 9925-9937.

[71] A Kafesa, W Darmanto and SPW Wahyuningsih. Silver nanoparticles with modified synthesis use sodium borohydride reducing agent and okra (*Abelmoschus esculentus* L.) raw polysaccharide extract as an anti-colon cancer. *Trends in Sciences* 2024; **21(11)**, 8149.

[72] E Ahmadian, SM Dizaj, E Rahimpour, A Hasanzadeh, A Eftekhari, J Halajzadeh and H Ahmadian. Effect of silver nanoparticles in the induction of apoptosis on human hepatocellular carcinoma (HepG2) cell line. *Materials Science and Engineering: C* 2018; **93**, 465-471.

[73] Z Wang, G Qu, L Su, L Wang, Z Yang, J Jiang, S Liu and G Jiang. Evaluation of the biological fate and the transport through biological barriers of nanosilver in mice. *Current Pharmaceutical Design* 2013; **19(37)**, 6691-6697.

[74] J Naik and M David. ROS mediated apoptosis and cell cycle arrest in human lung adenocarcinoma cell line by silver nanoparticles synthesized using *Swietenia macrophylla* seed extract. *Journal of Drug Delivery Science and Technology* 2023; **80**, 104084.

[75] MC Barton and G Lozano. p53 activation paradoxically causes liver cancer. *Cancer Research* 2022; **82(16)**, 2824-2825.

[76] M Isaq, YL Ramachandra, PS Rai, A Chavan, R Sekar, MJ Lee and P Somu. Biogenic synthesized silver nanoparticles using fungal endophyte *Cladosporium oxysporum* of *Vateria indica* induce apoptosis in human colon cancer cell line via elevated intracellular ROS generation and cell cycle arrest. *Journal of Molecular Liquids* 2023; **386**, 122601.

[77] A El-Hussein, I Mfouo-Tynga, M Abdel-Harith and H Abrahamse. Comparative study between the photodynamic ability of gold and silver nanoparticles in mediating cell death in breast and lung cancer cell lines. *Journal of Photochemistry and Photobiology B: Biology* 2015; **153**, 67-75.

[78] F Fontana, G Giannitti, S Marchesi and P Limonta. The PI3K/Akt pathway and glucose metabolism: a dangerous liaison in cancer. *International Journal of Biological Sciences* 2024; **20(8)**, 3113-3134.

[79] PS Mundi, J Sachdev, C McCourt and K Kalinsky. AKT in cancer: New molecular insights and advances in drug development. *British Journal of Clinical Pharmacology* 2016; **82(4)**, 943-956.

[80] MR Mohamed, SA Osman, AA Hassan, AI Raafat, MM Refaat and SA Fathy. Gemcitabine and synthesized silver nanoparticles impact on chemically induced hepatocellular carcinoma in male rats. *International Journal of Immunopathology and Pharmacology* 2024. https://doi.org/10.1177/03946320241263352

[81] NA Azhar, SZ Ghozali, SAA Bakar, V Lim and NH Ahmad. Suppressing growth, migration, and invasion of human hepatocellular carcinoma HepG2 cells by *Catharanthus roseus*-silver nanoparticles. *Toxicology in Vitro* 2020; **67**, 104910.

[82] SJ Wu, LT Ng and CC Lin. Cinnamaldehyde-induced apoptosis in human PLC/PRF/5 cells through activation of the proapoptotic Bcl-2 family proteins and MAPK pathway. *Life Sciences* 2005; **77(8)**, 938-951.

[83] J Li, Y Teng, S Liu, Z Wang, Y Chen, Y Zhang, S Xi, S Xu, R Wang and X Zou. Cinnamaldehyde affects the biological behavior of human colorectal cancer cells and induces apoptosis via inhibition of the PI3K/Akt signaling pathway. *Oncology Reports* 2016; **35(3)**, 1501-1510.

[84] OV Morozova. Silver nanostructures: limited sensitivity of detection, toxicity and anti-inflammation effects. *International Journal of Molecular Sciences* 2021; **22(18)**, 9928.

[85] YP Hsiao, WW Lai, SB Wu, CH Tsai, SC Tang, JG Chung and JH Yang. Triggering apoptotic death of human epidermal keratinocytes by malic Acid: Involvement of endoplasmic reticulum stress-and mitochondria-dependent signaling pathways. *Toxins* 2015; **7(1)**, 81-96.

[86] N Khurana, MPS Ishar, A Gajbhiye and RK Goel. PASS assisted prediction and pharmacological evaluation of novel nicotinic analogs for nootropic activity in mice. *European Journal of Pharmacology* 2011; **662(1-3)**, 22-30.

[87] B Chand. Structure–bioactivity-relationships and crystallographic analysis of secondary interactions in pregnane-based steroids. *Journal of Chemical Crystallography* 2011; **41(12)**, 1901-1926.

[88] DM Hasyim, I Musfiroh, R Hendra, TM Fakih, NKK Ikram and M Muchtaridi. *In silico* approaches for the discovery of novel pyrazoline benzenesulfonamide derivatives as anti-breast cancer agents against Estrogen receptor alpha (ERα). *Applied Sciences* 2025; **15(15)**, 8444.

[89] G Mustafa, HS Mahrosh, M Zafar, SA Attique and R Arif. Exploring the antihyperglycemic potential of tetrapeptides devised from AdMc1 via different receptor proteins inhibition using *in silico* approaches. *International Journal of Immunopathology and Pharmacology* 2022. https://doi.org/10.1177/03946320221103120

[90] AI Dara and P Husni. Teknik meningkatkan kelarutan obat (*In Indonesian*). *Farmaka* 2017;

**15(4)**, 49-57.

[91] J Baell, M Congreve, P Leeson and C Abad-Zapatero. Ask the experts: past, present and future of the rule of five. *Future Medicinal Chemistry* 2013; **5(7)**, 745-752.

[92] OA Raevsky, VI Fetisov, EP Trepalina, JW McFarland and KJ Schaper. Quantitative estimation of drug absorption in humans for passively transported compounds on the basis of their physico-chemical parameters. *Quantitative Structure-Activity Relationships* 2000; **19(4)**, 366-374.

[93] DR Dwijayanti, A Mamamia, RYN Maulana, N Rosyadah and N Widodo. Beyond a spice: harnessing the anti-inflammatory potential of Indonesian ginger−insights into gingerenones and isogingerenone. *Cogent Food & Agriculture* 2025; **11(1)**, 2568198.

[94] H Wang, M Guo, H Wei and Y Chen. Targeting p53 pathways: mechanisms, structures and advances in therapy. *Signal Transduction and Targeted Therapy* 2023; **8(1)**, 92.

[95] B Ahmed, S Khan, F Nouroz, U Farooq and S Khalid. Exploring multi-target inhibitors using *in silico* approach targeting cell cycle dysregulator–CDK proteins. *Journal of Biomolecular Structure and Dynamics* 2022; **40(19)**, 8825-8839.

[96] XH Xia, X Dai, H Yu, S Zhou, Z Fan, G Wei, Q Tang, Q Gong and F Bi. EGFR-PI3K-PDK1 pathway regulates YAP signaling in hepatocellular carcinoma: the mechanism and its implications in targeted therapy. *Cell Death & Disease* 2018; **9(3)**, 269.

[97] T Couri and A Pillai. Goals and targets for personalized therapy for HCC. *Hepatology International* 2019; **13(2)**, 125-137.

[98] SA Khan and TKW Lee. Investigations of nitazoxanide molecular targets and pathways for the treatment of hepatocellular carcinoma using network pharmacology and molecular docking. *Frontiers in Pharmacology* 2022; **13**, 968148.

[99] AS Alanazi, TO Mirgany, AA Alsfouk, NA Alsaif and MM Alanazi. Antiproliferative activity, multikinase inhibition, apoptosis-inducing effects and molecular docking of novel isatin–purine hybrids. *Medicina* 2023; **59(3)**, 610.